Journal of Applied Physics ARTICLE scitation.org/journal/jap

Robustness of semimetallic transport properties of TaAs against off-stoichiometric disorder

Cite as: J. Appl. Phys. 133, 223903 (2023); doi: 10.1063/5.0147663
Submitted: 24 February 2023 · Accepted: 22 May 2023 ·
Published Online: 8 June 2023

A. Kawasuso,[1,a)] M. Suda,[2] H. Murakawa,[3] M. Komada,[3] C. Suzuki,[1] H. Amada,[1] K. Michishio,[4] M. Maekawa,[1] A. Miyashita,[1] N. Seko,[1] S. Yamamoto,[1] N. Oshima,[4] S. Seki,[2] and N. Hanasaki[3]

AFFILIATIONS

[1]National Institute for Quantum Science and Technology, 1233 Watanuki, Takasaki, Gunma 370-1292, Japan
[2]Kyoto University, Nishikyo-ku, Kyoto-shi, Kyoto 615-8510, Japan
[3]Osaka University, 1-1 Machikaneyama, Toyonaka, Osaka 560-0043, Japan
[4]National Institute of Advanced Industrial Science and Technology (AIST), 1-1-1 Umezono, Tsukuba, Ibaraki 305-8568, Japan

[a)]**Author to whom correspondence should be addressed:** kawasuso.atsuo@qst.go.jp

ABSTRACT

TaAs single crystals were grown by a standard chemical vapor transport method. The single-crystallinity and homogeneous distribution of elements were confirmed by transmission electron microscope and x-ray diffraction observations. Positron annihilation measurements revealed that the atomic vacancy concentration was kept below 10^{-5} at. %. However, inductively coupled plasma analysis showed an As-deficient (7–9 at. %) off-stoichiometry. First-principles calculations implied that the off-stoichiometry could be compensated for with excess Ta antisite defects, thereby inducing metallic states. Nevertheless, excellent semimetallic transport properties of a well-suppressed carrier density ($\lesssim 10^{18}$ cm^{-3}), ultrahigh carrier mobility ($\gtrsim 10^{6}$ cm^2/V/s), and large transverse magnetoresistance (>200 000% at 9 T) with the quantum oscillation were obtained at 1.7 K. This indicated the robustness of semimetallic transport properties against the off-stoichiometric disorder and the quenching of metallic conduction associated with excess Ta atoms. The negative longitudinal magnetoresistance, which is considered evidence of a Weyl semimetal (chiral anomaly), was not observed. These data were discussed with theoretical calculations.

I. INTRODUCTION

Some pnictide semimetals, including TaAs, have been theoretically predicted to host Weyl fermions,[1] characterized by the formation of multiple Weyl node pairs of linear dispersions with opposite chirality near the Fermi level. The inversion/time-reversal symmetry breaking and strong spin–orbit interaction are the sources of this unusual electronic state.[2] The characteristics of the Fermi surface topology including a Fermi arc were identified for stoichiometric TaAs by photoemission spectroscopy.[3–6] Negative longitudinal magnetoresistance (MR) is also expected to appear due to the chiral anomaly of the Weyl system,[7,8] in addition to usual semimetallic transport properties, such as ultrafast carrier mobility and large transverse MR. These features have also been confirmed experimentally.[9–11]

Although real crystals usually contain some disorder, such as atomic exchange among different sublattices and structural and thermal equilibrium point defects, disorder has not been adequately investigated experimentally in Weyl systems. In a disordered Weyl system, finite states may be induced near the Fermi level, changing the system from a semimetal to a metal. The robustness of Weyl fermions against disorder needs to be explored.[12,13]

Structural analyses are important for examining the effects of disorder on Weyl fermions. In this study, we grew TaAs single crystals by the standard chemical vapor transport (CVT) method. We performed structural and compositional analyses by transmission electron microscopy (TEM), x-ray diffraction (XRD), positron annihilation, and inductively coupled plasma (ICP), as well as magnetotransport measurements. The results suggested that the semimetallic magnetotransport properties of TaAs are robust against As-deficient off-stoichiomeric disorder.

II. METHODS

The TaAs bulk crystals were grown by the CVT method.[14,15] Ta foil (99.95%), As grains (99.999%), and iodine (99.999%) were put into an evacuated silica tube (2 cm in diameter and 25 cm long). CVT growth was achieved by applying a temperature

gradient of 1050–980 °C over 3 weeks. The sample crystallinity was determined by TEM and XRD measurements. Spatial distributions of elements were visualized by energy-dispersive x-ray (EDX) analysis in the TEM apparatus. ICP analysis was used to determine the stoichiometry precisely. The inclusion of vacancy defects was also examined by positron annihilation measurements with monoenergetic positron beams.[16–18] Finally, magnetotransport measurements were conducted at 1.7–300 K by the four-probe method in the (001) plane. The sample dimension (width×thickness×length) was 0.51 × 0.66 × 1.78 mm.

To discuss the experimental data, density functional theory (DFT) calculations were performed by using the ABINIT code[19] with the projector augmented-wave method[20] within the generalized gradient approximation.[21] A conventional 2 × 2 × 1 cell ($Ta_{16}As_{16}$) was constructed for a perfect TaAs crystal. Systems with a Ta single vacancy ($Ta_{15}As_{16}$), As single vacancy ($Ta_{16}As_{15}$), Ta antisite ($Ta_{17}As_{15}$), and As antisite ($Ta_{15}As_{17}$) were also modeled. Full structural optimization was performed starting from the experimental lattice constants ($a = 3.44$ Å and $c = 11.66$ Å).[22] The valence electron configurations were assumed to be $5s^25p^65d^36s^2$ (Ta) and $3d^{10}4s^24p^3$ (As). Defect formation energies were calculated as $E_f = E_{tot}(\text{Defect}) - E_{tot}(\text{Perfect}) - \sum n_i\mu_i$, where E_{tot} is the total energy, n_i is the number of atoms i to be removed (<0) or added (>0), and μ_i is the chemical potential. Positron wave functions were obtained through two-component DFT.[23] The Slater functions[24] were used as core electron wave functions. The Borónski–Nieminen (BN)[23] and Barbiellini–Puska–Torsti–Nieminen (BPTN)[25] enhancement factors were used to simulate the electron-positron correlation effect. The positron lifetime and Doppler broadening of annihilation radiation (DBAR) spectra were calculated. The DBAR spectra were convoluted with the Gaussian resolution function with a full width at half maximum of 5.488×10^{-3} m_0c.

III. RESULTS

A. Structural analyses

The picture in Fig. 1(a) shows a crystal with major facets of the (001), (101), and (112) planes. The typical crystal size varied from 1 to 5 mm. Figure 1(a) also shows the x-ray diffraction intensity curves at the θ–2θ configuration for each facet. These indicated a single crystal with a body-centered tetragonal structure (space group: $I4_1md$, No. 109). Figures 1(b) and 1(c) show a TEM image and electron diffraction pattern, respectively, that contain clear lattice fringes and sharp diffraction spots, again confirming that a single crystal was obtained. Stacking faults were not observed.[15,26]

Figure 1(d) shows the EDX profiles of Ta and As atoms, suggesting a homogeneous distribution of these elements. Generally, EDX cannot determine the precise composition, even at the atomic percent level. Here, we used ICP analysis for randomly selected two pieces of TaAs crystals. The result showed 7%–9% As-deficient off-stoichiometry, as listed in Table I. This is the largest off-stoichiometry ever reported for TaAs. Such an As-deficiency was probably due to the high vapor pressure of As.

To reveal the inclusion of structural vacancies compensating for the 7–9% off-stoichiometry, positron annihilation measurements were conducted. Figure 2(a) shows the positron lifetime spectrum after subtracting the instrumental component (510 ps, 10%).

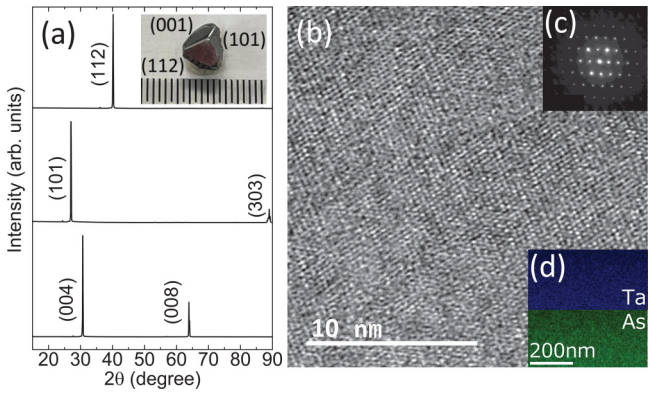

FIG. 1. Structural analyses of the present TaAs crystal. (a) XRD patterns from the (112), (101), and (001) facets, (b) TEM images, (c) electron diffraction pattern, and (d) two-dimensional EDX maps. The inset in (a) shows a picture of a typical crystal.

The experimental spectrum had longer lifetimes than the spectra simulated for the perfect matrix with positron lifetimes of 117 ps (BN) and 132 ps (BPTN) calculated by DFT, indicating the inclusion of atomic vacancies. The spectrum was fitted with a dual-exponential function [$\sum I_i\exp(-t/\tau_i)/\tau_i$, where τ_i and I_i ($i = 1, 2$) are the lifetime and intensity, respectively]. The first lifetime, τ_1, was assigned to the reduced bulk lifetime due to the finite positron trapping rate of vacancies.[16] The vacancy-related lifetime was $\tau_2 = 181$ ps with $I_2 = 59\%$, which was closer to the calculated values for Ta vacancy (163–199 ps) than to those for As vacancy (148–164 ps), where the lower and higher values were based on the BN and BPTN enhancement factors, respectively. Figure 2(b) shows the DBAR spectrum, where the gamma-ray energy is converted to the electron momentum. The comparison with the calculation indicated the inclusion of single vacancies. However, the vacancy concentration was below $\sim 10^{-5}$ at. % (10 ppm) because the intensity related to vacancies (55%–59%) was still below the saturation limit. Therefore, the most important conclusion was that the 7%–9% As deficiency was not compensated for by the formation of vacancies, and thus the presence of excess Ta antisite defects was suspected.

B. Magnetotransport measurements

Figure 3(a) shows the temperature dependence of the longitudinal resistivity (ρ_{xx}). At a zero field, ρ_{xx} increased upon heating, suggesting that phonon scattering was the major cause of resistivity. The residual resistance ratio of 1.7 K vs 300 K was 31.

Figure 3(b) (upper panels) shows the Hall resistivity (ρ_{xy}) as a function of magnetic field at different temperatures. Below 50 K, the slopes were negative overall with a quantum oscillation. Above

TABLE I. ICP compositional analysis of two TaAs crystals in the same batch.

No. 1	Ta:	59.00%	As:	41.00%
No. 2	Ta:	57.14%	As:	42.86%

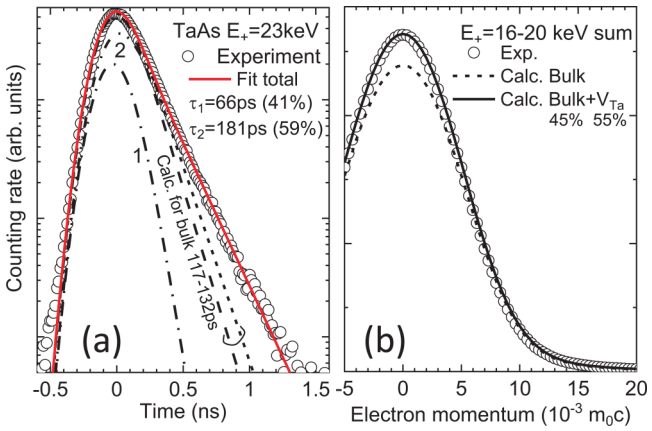

FIG. 2. (a) Positron annihilation lifetime spectrum obtained for the present TaAs crystal at an incident positron energy of $E_+ = 23$ keV (open circles). Simulated spectra with the positron bulk (perfect matrix) lifetimes calculated by DFT with the BN (broken line) and BPTN (short-broken line) enhancement factors. Fitted curve assuming a dual-exponential function (solid line) and the individual components (one- and two-dotted chain lines denoted as 1 and 2, respectively) with their lifetimes (τ_1 and τ_2) and intensities are shown. (b) DBAR positron spectrum obtained for the present TaAs crystal summed over $E_+ = 16$–20 keV (open circles). Spectra for the bulk (broken line) and bulk with a Ta single vacancy (solid line) calculated by DFT are shown.

100 K, the slopes were positive and the absolute values were two orders of magnitude smaller than those above 50 K. These results suggested that the electrons were the main carriers at low temperatures, whereas the holes took over at high temperatures. Focusing on the lowest temperature (1.7 K), the analysis based on the two-carrier model assuming both electrons and holes ($\sigma_{xy} = \rho_{xy}/(\rho_{xy}^2 + \rho_{xx}^2)$ $= eB[n_h\mu_h^2/\{1 + (\mu_h B)^2\} - n_e\mu_e^2/\{1 + (\mu_e B)^2\}]$, where $n_{e(h)}$, $\mu_{e(h)}$, B and e denote the electron (hole) density and mobility, magnetic field and elementary charge, respectively) gave $n_e = 4.0 \times 10^{17}$ cm^{-3}, $\mu_e = 1 \times 10^6$ cm^2/V/s, $n_h = 2.5 \times 10^{17}$ cm^{-3}, and $\mu_h = 5 \times 10^4$ cm^2/V/s as in the previous works.[9–11]

Figure 3(b) (lower left panel) shows the transverse MR values ($[\rho_{xx}(B) - \rho_{xx}(0)]/\rho_{xx}(0)$) at $\vec{B} \perp \vec{I}$, where $\vec{B}$ and $\vec{I}$ denote the magnetic field and current vectors, respectively, and at different temperatures. Below 20 K, the transverse MR values were over 200 000% at 9 T, and the quantum oscillation again appeared. Figure 3(b) (lower right panel) shows the longitudinal MR values at around $\vec{B} \parallel \vec{I}$. Although the MR values were largely suppressed from $\vec{B} \perp \vec{I}$ to $\vec{B} \parallel \vec{I}$, the positive sign still remained.

Figure 3(c) shows the oscillatory spectrum of transverse MR ($\Delta\rho_{xx}$) at 1.7 K by subtracting the MR curve at 20 K as a function of inverse of magnetic field (B^{-1}). As indicated by arrows, two oscillation frequencies [$F = 7.0$ T (A) and 13.2 T (B)] could be specified. The maximal cross sections of the Fermi surfaces were estimated to be $A_F = 6.7 \times 10^{-4}$ Å^{-2} for A and $A_F = 1.26 \times 10^{-3}$ Å^{-2} for B with $A_F = 2\pi eF/\hbar$, where $\hbar$ is the Planck constant. These might correspond to the theoretical values for one of the Weyl-type electron pockets and the hole poket, respectively.[27] As shown in Fig. 3(c), the oscillatory spectrum could also be fitted with the Lifshits–Kosevich

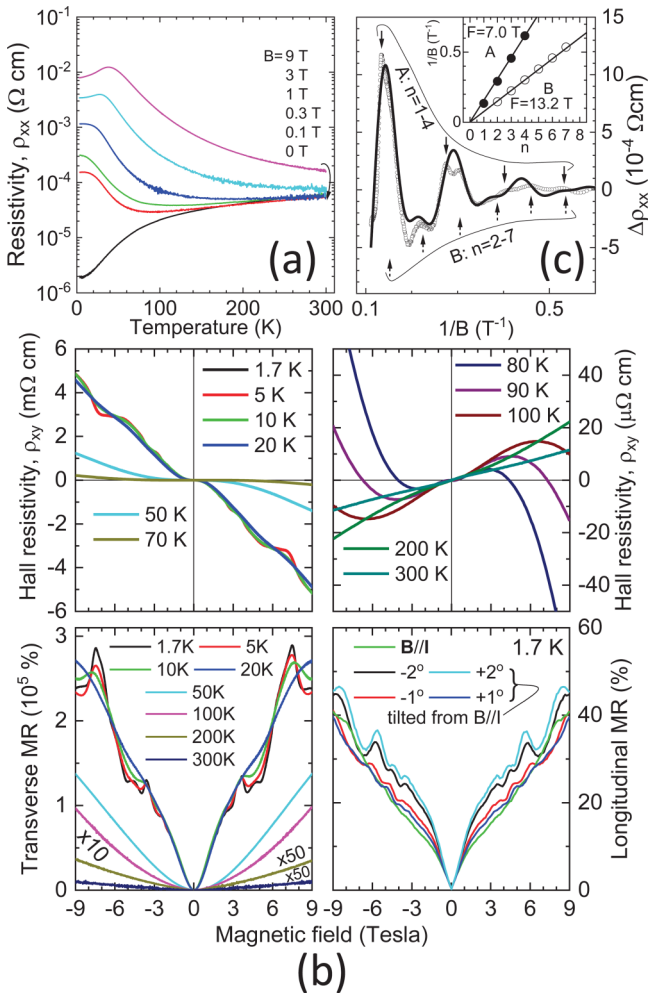

FIG. 3. (a) Longitudinal resistivity as a function of temperature, (b) Hall resistivity (upper two panels), transverse ($\vec{B} \perp \vec{I}$) magnetoresistances (lower left panel) and longitudinal ($\vec{B} \parallel \vec{I}$) magnetoresistances (lower right panel) in the magnetic field of −9 to +9 T at different temperatures and (c) the oscillatory spectrum of transverse MR (open circles) at 1.7 K as a function of B^{-1} obtained for the present TaAs. In (c), arrows indicate the peak positions of two oscillation components designated by their frequencies, A (7.0 T) and B (13.2 T), and the Landau level indices(n). The solid line is the fitting by the Lifshitz–Kosevich formula, and the inset shows the peak position ($1/B$) vs n plots.

formula,[9,10,28] $MR \propto \exp(-\alpha)\beta/\sinh(\beta)\cos\{2\pi(F/B + \gamma)\}$ with $\alpha = 2\pi^2 k_B T_D m_{cyc}/(eB\hbar)$ and $\beta = 2\pi^2 k_B T m_{cyc}/(eB\hbar)$, where k_B, T_D, γ, m_{cyc}, and T denote the Boltzmann constant, the Dingle temperature, the Onsager phase factor, cyclotron mass and temperature, respectively. The peak position vs Landau-level index plot in the inset of Fig. 3(c) suggested that the Onsager phase factor may be 0 or 1. From the temperature-dependent amplitude of $n = 1$ for A at 1.7–10 K, the cyclotron mass was determined to be $m_{cyc} = 0.096\, m_0$, where m_0 is the electron rest mass. Subsequently, using this value, the Dingle temperature was determined to be $T_D = 8.0$ K at 1.7 K.

The Fermi vector, the Fermi velocity, the scattering time constant and eventually the mean free path were estimated to be $k_F = (A_F/\pi)^{1/2} = 0.015$ Å^{-1}, $v_F = \hbar k_F/m_{cyc} = 1.7 \times 10^7$ cm/s, $\tau_{tr} = \mu\hbar k_F/(ev_F) = 5.4 \times 10^{-11}$ s, and $l = v_F\tau_{tr} = 9.2\,\mu$m, respectively.

The above-observed ultrahigh mobility, well-suppressed carrier density, giant transverse MR, and the deduced physical quantities through the analyses were comparable to those obtained for stoichiometric TaAs in the previous works,[9,10] suggesting the presence of Weyl semimetallicity even in the off-stoichiometric case. The one missing observation was of the negative longitudinal MR, which is considered to be the signature of Weyl characteristics due to chiral anomaly.

IV. DISCUSSION

The present TaAs crystals were highly homogeneous single crystals with 7%–9% As-deficient off-stoichiometry and few structural vacancies. The present DFT calculation gave the formation energies of vacancies and antisite defects as 3.7 eV (Ta vacancy), 4.0 eV (As vacancy), 3.5 eV (Ta antisite), and 4.4 eV (As antisite). The value for As vacancy agreed with that calculated in the previous study.[26] These high formation energies implied that TaAs contains few point defects even at 1000 °C, as long as it is stoichiometric. According to the grand canonical theory on point defect formation in binary alloys,[29] Ta antisite defects are probably formed in As-deficient conditions. The present TaAs may correspond to this case.

The modification of the electronic states of TaAs by point defects may be a concern. Figure 4 shows the DFT calculation of the electron density of states (DOS) for pristine TaAs and with single vacancies and antisite defects on both sublattices. The concentration of these point defects was 3.125 at. % (=1/32). The minimum DOS point (Weyl node) for the pristine TaAs was located at the Fermi level (0 eV). The DOS profile around the Fermi level exhibited linear dispersion. The minimum DOS points for the As vacancies and Ta antisites were slightly below the Fermi level, whereas those for Ta vacancies and As antisites were shifted above the Fermi level. These tendencies were explained qualitatively by considering the difference in the electronegativities of Ta (1.5) and As (2.18) atoms, and hence the ionicity in the crystal bonding. That is, As (Ta) vacancies and Ta (As) antisite defects have a positive (negative) effective charge and dope electrons (holes) to maintain the charge neutrality of the system. Therefore, the Fermi level tended to shift upwards (As vacancy and Ta antisite) or downwards (Ta vacancy and As antisite). In all cases, finite states were created at the Fermi level, as seen in Fig. 4, and thus metallic conduction could appear.

However, the present transport measurements (Fig. 3) showed no metallic conduction. The off-stoichiometry seemed to cause no serious degradation of the semimetallic transport properties compared with TaAs crystals reported to be stoichiometric.[9,10] Therefore, even though the off-stoichiometry created states near the Fermi level, they hardly generated metallic conduction (i.e., quenched), for instance, due to the Anderson localization below the mobility edge. Furthermore, the semimetallic transport properties of TaAs were robust against the disorder created by excess Ta antisite defects. The

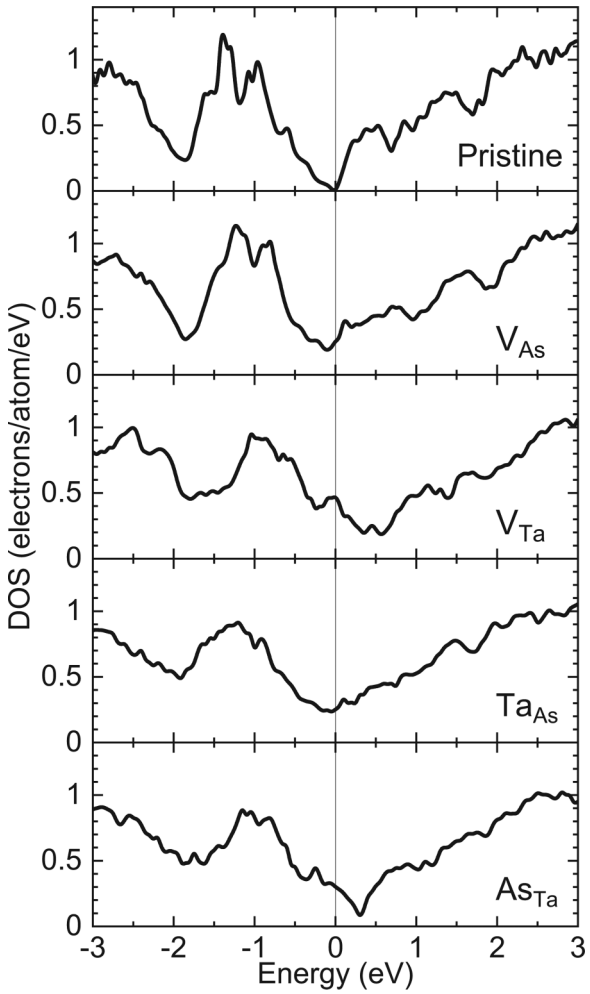

FIG. 4. Electron DOS for pristine TaAs crystal and TaAs crystals containing 3.125 at. % As, Ta vacancies (V_{As}, V_{Ta}), and antisites (Ta_{As}, As_{Ta}) calculated by DFT using 2 × 2 × 1 conventional cells. The Fermi level is located at 0 eV.

above scenario agreed with the theoretical prediction of the conservation of ballistic transport of Weyl fermions in disordered systems.[12,13] The theory suggests that linear dispersion plays an essential role. The robustness of ultrahigh mobility against impurities has also been proposed in intentionally doped NbP.[30] To pursue the robustness of semimetallic transport properties of TaAs against off-stoichiometric disorder more in detail, the Ta/As ratio should be controlled more systematically in future.

As for the absence of negative longitudinal MR in the present TaAs, a technical problem is first considered. In TaAs, an extremely large positive transverse MR may disturb the relatively weak negative longitudinal MR, even for a small misalignment of current and field directions.[9] This explanation has also been proposed in the context of the current jet effect.[2] Excess Ta anitisite defects may also degrade weak negative longitudinal MR through carrier

scattering among valleys of opposite chirality.[31,32] Lastly, we discuss the negative longitudinal MR from a general viewpoint. Although this effect is thought to be evidence for the chiral anomaly of Weyl fermions, there are other channels that can produce negative longitudinal MR. For example, negative longitudinal MR can be induced through the unentanglement of weakly localized disorder (i.e., quenched metallic states) with the magnetic field.[33] Anisotropic DOS can also induce negative longitudinal MR in magnetic systems.[34] Considering that negative longitudinal MR is widely observed in magnetic Weyl systems (Co_2MnGa[35] and Mn_3Sn[36]), and also in non-Weyl systems, such as $TaAs_2$,[37,38] it is still uncertain whether this effect could be evidence of the chiral anomaly of Weyl fermions.[2]

V. CONCLUSION

We investigated CVT-grown TaAs single crystals via structural analyses and magnetotransport measurements. The crystals had high single-crystalline order and 7%–9% As-deficient off-stoichiometry. Excess Ta atoms due to the off-stoichiometry were considered to form Ta antisite defects rather than As vacancies. No metallic conduction was caused by the off-stoichiometric disorder; that is, metallic states might be quenched for some reason. The robustness of the excellent semimetallic transport properties against off-stoichiometric disorder may be promising in future device applications.

ACKNOWLEDGMENTS

The authors thank K. Kobayashi of Kyushu University for fruitful discussion. This work was financially supported by a JSPS KAKENHI Grant-in-Aid for Scientific Research (B) (No. JP21H03748) and partly supported by MEXT ARIM (No. JPMXP1222AT5020).

DATA AVAILABILITY

The data that support the findings of this study are available within the article.

AUTHOR DECLARATIONS

Conflict of Interest

The authors have no conflicts to disclose.

Author Contributions

A. Kawasuso: Conceptualization (equal); Data curation (equal); Formal analysis (equal); Funding acquisition (equal); Investigation (equal); Methodology (equal); Project administration (equal); Resources (equal); Software (equal); Supervision (equal); Validation (equal); Visualization (equal); Writing – original draft (equal); Writing – review & editing (equal). **M. Suda:** Data curation (equal); Formal analysis (equal); Investigation (equal); Methodology (equal); Software (equal); Validation (equal). **H. Murakawa:** Data curation (equal); Investigation (equal); Methodology (equal); Validation (equal). **M. Komada:** Methodology (lead). **C. Suzuki:** Formal analysis (lead). **H. Amada:** Formal analysis (lead). **K. Michishio:** Data curation (lead); Formal analysis (lead). **M. Maekawa:** Funding acquisition (equal); Methodology (equal). **A. Miyashita:** Formal analysis (equal); Methodology (equal). **N. Seko:** Methodology (equal); Supervision (equal). **S. Yamamoto:** Formal analysis (equal); Methodology (equal). **N. Oshima:** Methodology (equal); Supervision (equal). **S. Seki:** Methodology (supporting); Supervision (equal). **N. Hanasaki:** Methodology (supporting); Supervision (equal).

REFERENCES

[1]H. Weng, C. Fang, Z. Fang, B. A. Bernevig, and X. Dai, Phys. Rev. X **5**, 011029 (2015).
[2]N. P. Armitage, E. J. Mele, and A. Vishwanath, Rev. Mod. Phys. **90**, 015001 (2018).
[3]B. Q. Lv, H. M. Weng, B. B. Fu., X. P. Wang, H. Miao, J. Ma, P. Richard, X. C. Huang, L. X. Zhao, G. F. Chen, Z. Fang, X. Dai, T. Qian, and H. Ding, Phys. Rev. X **5**, 031013 (2015).
[4]S. Y. Xu, N. Alidoust, I. Belopolski, Z. Yuan, G. Bian, T. R. Chang, H. Zheng, V. N. Strocov, D. S. Sanchez, G. Chang, C. Zhang, D. Mou, Y. Wu, L. Huang, C. C. Lee, S. M. Huang, B. Wang, A. Bansil, H. T. Jeng, T. Neupert, A. Kaminski, H. Lin, S. Jia, and M. Z. Hasan, Science **349**, 613 (2015).
[5]L. X. Yang, Z. K. Liu, Y. Sun, H. Peng, H. F. Yang, T. Zhang, B. Zhou, Y. Zhang, Y. F. Guo, M. Rahn, D. Prabhakaran, Z. Hussain, S.-K. Mo, C. Felser, B. Yan, and Y. L. Chen, Nat. Phys. **11**, 728 (2015).
[6]F. Arnold, M. Naumann, S. C. Wu, Y. Sun, M. Schmidt, H. Borrmann, C. Felser, B. Yan, and E. Hassinger, Phys. Rev. Lett. **117**, 146401 (2016).
[7]A. A. Burkov, Phys. Rev. Lett. **113**, 247203 (2014).
[8]D. T. Son and B. Z. Spivak, Phys. Rev. B **88**, 104412 (2013).
[9]X. Huang, L. Zhao, Y. Long, P. Wang, D. Chen, Z. Yang, H. Liang, M. Xue, H. Weng, Z. Fang, X. Dai, and G. Chen, Phys. Rev. X **5**, 031023 (2015).
[10]C. L. Zhang, S. Y. Xu, I. Belopolski, Z. Yuan, Z. Lin, B. Tong, G. Bian, N. Alidoust, C. C. Lee, S. M. Huang, T. R. Chang, G. Chang, C. H. Hsu, H. T. Jeng, M. Neupane, D. S. Sanchez, H. Zheng, J. Wang, H. Lin, C. Zhang, H. Z. Lu, S. Q. Shen, T. Neupert, M. Z. Hasan, and S. Jia, Nat. Commun. **7**, 10735 (2015).
[11]C. L. Zhang, Z. Yuan, Q. D. Jiang, B. Tong, C. Zhang, X. C. Xie, and S. Jia, Phys. Rev. B **95**, 085202 (2017).
[12]S. V. Syzranov, L. Radzihovsky, and V. Guraie, Phys. Rev. Lett. **114**, 166601 (2015).
[13]K. Kobayashi, M. Wada, and T. Ohtsuki, Phys. Rev. Res. **2**, 022061(R) (2020).
[14]Z. Li, H. Chen, S. Jin, D. Gan, W. Wang, L. Guo, and X. Chen, Cryst. Growth Des. **16**, 1172 (2016).
[15]R. Sankar, G. Peramaiyan, I. P. Muthuselvam, S. Xu, M. Z. Hasan, and F. C. Chou, J. Phys.: Condens. Matter **30**, 015803 (2018).
[16]R. Krause-Rehberg and H. S. Leipner, *Positron Annihilation in Semiconductors* (Springer, 1998).
[17]F. Tuomisto and I. Makkonen, Rev. Mod. Phys. **85**, 1583 (2013).
[18]N. Oshima, R. Suzuki, T. Ohdaira, A. Kinomura, T. Narumi, A. Uedono, and M. Fujinami, Appl. Phys. Lett. **94**, 194104 (2009).
[19]X. Gonze, J.-M. Beuken, R. Caracas, F. Detraux, M. Fuchs, G.-M. Rignanese, L. Sindic, M. Verstraete, G. Zerah, F. Jollet, M. Torrent, A. Roy, M. Mikami, P. Ghosez, J.-Y. Raty, and D. Allan, Comput. Mater. Sci. **25**, 478 (2002).
[20]P. E. Blöchl, Phys. Rev. B **50**, 17953 (1994).
[21]J. P. Perdew, K. Burke, and M. Ernzerhof, Phys. Rev. Lett. **77**, 3865 (1996).
[22]J. J. Murray, J. B. Taylor, L. D. Calvert, Y. Wang, E. J. Gabe, and J. Despault, J. Less Common Met. **46**, 311 (1976).
[23]E. Boroński and R. M. Nieminen, "Electron-positron density-functional theory," Phys. Rev. B **34**, 3820 (1986).
[24]E. Clementi and C. Roetti, At. Data Nucl. Data Tables **14**, 177 (1974).
[25]B. Barbiellini, M. J. Puska, T. Torsti, and R. M. Nieminen, Phys. Rev. B **51**, 7341(R) (1995).
[26]T. Besara, D. A. Rhodes, K.-W. Chen, S. Das, Q. R. Zhang, J. Sun, B. Zeng, Y. Xin, L. Balicas, R. E. Baumbach, E. Manousakis, D. J. Singh, and T. Siegrist, Phys. Rev. B **93**, 245152 (2016).

[27]C. C. Lee, S. Y. Xu, S. M. Huang, D. S. Sanchez, I. Belopolsk, G. Chang, G. Bian, N. Alidoust, H. Zheng, M. Neupane, B. Wang, A. Bansil, M. Z. Hasan, and H. Lin, Phys. Rev. B **92**, 235104 (2015).
[28]H. Murakawa, M. S. Bahramy, M. Tokunaga, Y. Kohama, C. Bell, Y. Kaneko, N. Nagaosa, H. Y. Hwang, and Y. Tokura, Science **342**, 1490 (2013).
[29]M. Leitner, arXiv:1503.03798 (2015).
[30]Z. Wang, Y. Zheng, Z. Shen, Y. Lu, H. Hanyan, F. Sheng, Y. Zhou, X. Yang, Y. Li, C. Feng, and Z. A. Xu, Phys. Rev. B **93**, 121112(R) (2016).
[31]X. T. Ji, H. Z. Lu, Z. G. Zhu, and G. Su, J. Appl. Phys. **123**, 203901 (2018).
[32]X. T. Ji, H. Z. Lu, Z. G. Zhu, and G. Su, AIP Adv. **7**, 105003 (2017).
[33]P. A. Lee and T. V. Ramakrishnan, Rev. Mod. Phys. **57**, 287 (1985).
[34]S. Kokado, M. Tsunoda, K. Harigaya, and A. Sakuma, J. Phys. Soc. Jpn. **81**, 024705 (2012).
[35]A. Sakai, Y. P. Mizuta, A. A. Nugroho, R. Sihombing, T. Koretsune, M. Suzuki, N. Takemori, R. Ishii, D. Nishio-Hamane, R. Arita, P. Goswami, and S. Nakatsuji, Nat. Phys. **14**, 1119 (2018).
[36]K. Kuroda, T. Tomita, M.-T. Suzuki, C. Bareille, A. A. Nugroho, P. Goswami, M. Ochi, M. Ikhlas, M. Nakayama, S. Akebi, R. Noguchi, R. Ishii, N. Inami, K. Ono, H. Kumigashira, A. Varykhalov, T. Muro, T. Koretsune, R. Arita, S. Shin, T. Kondo, and S. Nakatsuji, Nat. Mater. **16**, 1090 (2017).
[37]Y. Luo, R. D. McDonald, P. F. S. Rosa, B. Scott, N. Wakeham, N. J. Ghimire, E. D. Bauer, J. D. Thompson, and F. Ronning, Sci. Rep. **6**, 27294 (2016).
[38]A. S. Wadge, G. Grabecki, C. Autieri, B. J. Kowalski, P. Iwanowski, G. Cuono, M. F. Islam, C. M. Canali, K. Dybko, A. Hruban, A. Łusakowski, T. Wojciechowski, R. Diduszko, A. Lynnyk, N. Olszowska, M. Rosmus, J. Kołodziej, and A. Wiśniewski, J. Phys.: Condens. Matter **34**, 125601 (2022).